Inorganic Chemistry

Article

pubs.acs.org/IC

Tunable-Color Luminescence via Energy Transfer in $NaCa_{13/18}Mg_{5/18}PO_4$:A (A = Eu^{2+}/Tb^{3+}/Mn^{2+}, Dy^{3+}) Phosphors for Solid State Lighting

Kai Li,[†,‡] Jian Fan,[§] Xiaoyun Mi,[†] Yang Zhang,[†,‡] Hongzhou Lian,*[,†] Mengmeng Shang,[†] and Jun Lin*[,†]

[†]State Key Laboratory of Rare Earth Resource Utilization, Changchun Institute of Applied Chemistry, Chinese Academy of Sciences, Changchun 130022, P. R. China

[‡]University of Chinese Academy of Sciences, Beijing 100049, P. R. China

[§]College of Chemical and Environmental Engineering, Shandong University of Science and Technology, Qingdao 266590, P. R. China

Supporting Information

ABSTRACT: A series of $NaCa_{13/18}Mg_{5/18}PO_4$(NCMPO):A (A = Eu^{2+}/Tb^{3+}/Mn^{2+}, Dy^{3+}) phosphors have been prepared by the high-temperature solid-state reaction method. The X-ray diffraction (XRD) and Rietveld refinement, X-ray photoelectron spectroscopy (XPS), photoluminescence (PL), cathodoluminescence (CL), decay lifetimes, and PL quantum yields (QYs) were utilized to characterize the phosphors. The pure crystalline phase of as-prepared samples has been demonstrated via XRD measurement and Rietveld refinements. XPS reveals that the Eu^{2+}/Tb^{3+}/Mn^{2+} can be efficiently doped into the crystal lattice. NCMPO:Eu^{2+}/Tb^{3+}/Mn^{2+} phosphors can be effectively excited under UV radiation, which show tunable color from purple-blue to red including white emission based on energy transfer from Eu^{2+} to Tb^{3+}/Mn^{2+} ions. Under low-voltage electron beam bombardment, the NCMPO:A (A = Eu^{2+}/Tb^{3+}/Mn^{2+}, Dy^{3+}) display their, respectively, characteristic emissions with different colors, and the CL spectrum of NCMPO:0.04Tb^{3+} has the comparable intensity to the ZnO:Zn commercial product. In addition, the calculated CIE coordinate of NCMPO:0.04Tb^{3+} (0.252, 0.432) is more saturated than it (0.195, 0.417). These results reveal that NCMPO:A (A = Eu^{2+}/Tb^{3+}/Mn^{2+}, Dy^{3+}) may be potential candidate phosphors for WLEDs and FEDs.

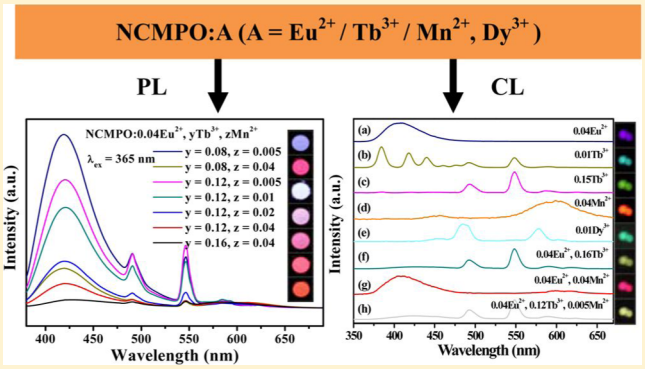

1. INTRODUCTION

Rare earth and transition metal ions (e.g., Mn^{2+}, Bi^{3+} etc.) doped inorganic luminescent materials have been attracting our attentions for their applications in fluorescent lamps (FLs), light-emitting diodes (LEDs), cathode ray tubes (CRTs) and field emission displays (FEDs) as indispensable components.[1] Currently, the issues of energy saving and environmental protection give a prompt development of LEDs for their unique merits such as high efficiency, long operation time, compactness, etc. besides energy saving and environmental friendliness compared to conventional incandescent and implemented fluorescent lamps.[2] Moreover, the commercial applications of LEDs have taken place as backlights for liquid crystal displays (LCDs), mobile phone screen, car taillight and so on. In the display field, the LCDs occupies the market at present; however, as the most potential technology for flat panel displays, FEDs owns many potential superiorities on lighting, viewing, operated-temperature range, power depletion, response time, and so on.[3] Therefore, the investigations devoted to them have attracted much interest from researchers.

It is well-known that energy transfer plays an important role to obtain tunable color emissions in many phosphors,[4] which can enrich the luminescent properties of samples and is beneficial for our selections we need. As an important activator for phosphors, Eu^{2+} can produce intensive and broad excitation and emission bands attributed to their dipole allowed 4f−5d electronic transitions. The emission wavelength can vary from n-UV to red region relying on various matrix, such as n-UV for $Na_2CaMg(PO_4)_2$:Eu^{2+}, blue for $BaCa_2MgSi_2O_8$:Eu^{2+}, green for $Li_2Ca_2Si_2O_7$:Eu^{2+}, yellow for $Sr_8MgGd(PO_4)_7$:Eu^{2+}, red for $CaAlSiN_3$:Eu^{2+}, and even full-color for $Na_{2-x}Al_{2-x}Si_xO_4$:Eu^{2+} ($0 < x < 1$).[5] The trivalent Tb^{3+} are usually used as a green emitting activator based on their characteristic transitions of $^5D_3 \rightarrow {}^7F_J$ in the n-UV to blue region and $^5D_4 \rightarrow {}^7F_J$ in the green region (J = 6, 5, 4, 3, 2) depending on its doping concentration.[6] The primary problem for the Tb^{3+} ion of its green emission is the deficiency of the efficient and broad

Received: August 23, 2014
Published: November 6, 2014

   dx.doi.org/10.1021/ic502058r | Inorg. Chem. 2014, 53, 12141−12150

excitation band from n-UV to the visible region, which limits its application in n-UV white LEDs (WLEDs). The transition metal ion Mn^{2+} can produce a broad band emission in the visible range from green to red depending on the around crystal field owing to its d-d transition. However, the d-d transition of Mn^{2+} is spin-forbidden and difficult to be pumped, therefore, the emission of Mn^{2+} ions can be generally enhanced by energy transfer from the host or the sensitizer.[7] Besides, Dy^{3+} ion can produce white light based on combination of blue ($^4F_{9/2}$-$^6H_{15/2}$ transition) and yellow ($^4F_{9/2}$-$^6H_{13/2}$ transition) emissions under UV excitation, which is also often used as an activator.[8]

$ABPO_4$ (where A and B are mono- and divalent cations, respectively), an important family of compounds showing excellent thermal and charge stability, have gained increasing interest in the investigations of luminescent materials, such as $NaCaPO_4:Ce^{3+},Tb^{3+}$, $RbBaPO_4:Eu^{2+}$, $NaCaPO_4:Mn^{2+}$, $NaSrPO_4:Eu^{2+}/Mn^{2+}$.[9] However, the structure of $NaCa_{13/18}Mg_{5/18}PO_4$ (NCMPO) (trigonal crystal structure) is much different from that of $NaCaPO_4$ (orthorhombic crystal structure), which may produce different luminescent properties when doped with rare earth ions and Mn^{2+} ions. In this present work, we have synthesized Eu^{2+}, Tb^{3+}, Mn^{2+}, Dy^{3+} doped NCMPO phosphors via the high-temperature solid-state reaction route. The tunable color from purple-blue to red has been produced via doping different kinds of ions and appropriately adjusting their doping concentration ratios under UV excitation. Simultaneously, the cathodoluminescence (CL) properties of phosphors also have been investigated in detail under a low voltage electron beam excitation to recognize their potential application in FEDs. Additionally, it develops that the new crystal structure can be produced when part of certain elements in some familiar compounds are substituted by other ones, which may give us an additional way to obtain novel phosphors.

2. EXPERIMENTAL SECTION

2.1. Materials and Preparation. A series of phosphors with the composition formula $NaCa_{13/18}Mg_{5/18}PO_4$ (NCMPO):$Eu^{2+}/Tb^{3+}/Mn^{2+}$, Dy^{3+} were prepared by the high-temperature solid-state reaction process. The Na_2CO_3 (A.R.), $CaCO_3$ (A.R.), $(MgCO_3)_4{\cdot}Mg(OH)_2{\cdot}5H_2O$ (A.R.), $NH_4H_2PO_4$ (A.R.), Eu_2O_3 (99.99%), Tb_4O_7 (99.99%), $MnCO_3$ (A.R.), and Dy_2O_3 (99.99%) were used as the starting materials. The stoichiometric amounts of the raw materials were first thoroughly mixed by grinding them in an agate mortar with an appropriate amount of ethanol and then dried at 80 °C for 0.5 h. After reground for 5 min, the powder mixtures were loaded into the crucibles and transferred to the tube furnace to calcine at 1030 °C for 7 h in a reducing atmosphere of H_2 (10%) and N_2 (90%) to produce the final samples after reground for 1 min.

2.2. Measurement Characterization. The X-ray diffraction (XRD) patterns were performed on a D8 Focus diffractometer at a scanning rate of 10° min^{-1} in the 2θ range from 10° to 120° with graphite-monochromatized Cu Kα radiation (λ = 0.15405 nm). X-ray photoelectron spectroscopy (XPS) spectra were measured with a Thermo ESCALAB 250 instrument. Diffuse reflectance spectra were recorded with a Hitachi U-4100-Vis/NIR spectrophotometer. The photoluminescence (PL) and CL emission spectra were recorded with a Hitachi F-7000 spectrophotometer with different excitation source (a 150 W xenon lamp and electron beam, respectively). The CL measurements were conducted in an ultrahigh vacuum chamber ($<10^{-8}$ Torr), where the phosphors were excited by an electron beam in the voltage range of 1.5−4.5 kV and different filament currents of 82−90 mA. The fluorescent decay lifetimes were measured from a Lecroy Wave Runner 6100 digital osilloscope (1 GHz) using a tunable laser (pulse width = 4 ns, gate = 50 ns) as the excitation source (Continuum Sunlite OPO). PL quantum yields (QYs) were obtained directly by the absolute PL quantum yield (internal quantum efficiency) measurement system (C9920-02, Hamamatsu Photonics K. K., Japan), including an excitation light source of a Xe lamp, a monochromator, an integrating sphere capable of nitrogen gas flow, and a CCD spectrometer for detecting the whole spectral range simultaneously. All the measurements were conducted at room temperature (RT).

3. RESULTS AND DISCUSSION

3.1. Crystal Structure and Phase Purity. The composition and phase purity of as-prepared samples were first identified by XRD measurement. Figure 1 illustrates the representative XRD patterns of NCMPO and Eu^{2+}, Tb^{3+}, Mn^{2+}, Dy^{3+} doped NCMPO samples as well as the reference diffraction lines of $Na_{18}Ca_{13}Mg_5(PO_4)_{18}$ (JCPDS no. 88-1548). It is apparent that all the diffraction peaks are well assigned to pure trigonal [space group, $R\bar{3}m$ (166)] based on the JCPDS no. 88-1548, which indicates Eu^{2+}, Tb^{3+}, Mn^{2+}, and Dy^{3+} ions can be dissolved into this host and their introductions do not arouse any significant changes in this crystal structure. As depicted in Figure 2, $Na_{18}Ca_{13}Mg_5(PO_4)_{18}$ crystallizes in the trigonal space group $R\bar{3}m$ with a relatively large unit cell and

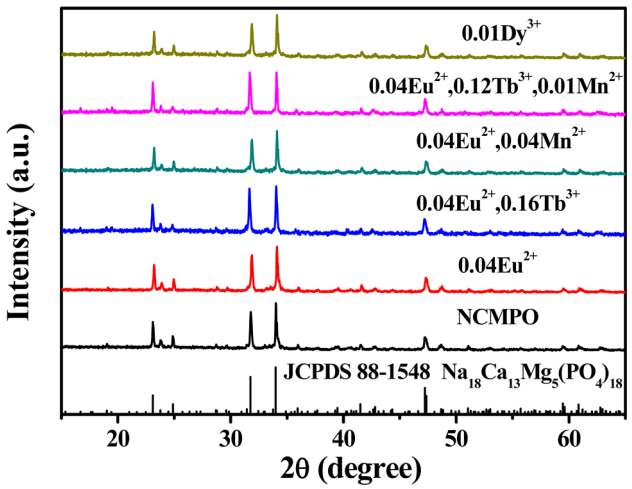

Figure 1. Representative XRD patterns for NCMPO, NCMPO:0.04Eu^{2+}, NCMPO:0.04Eu^{2+}, 0.16Tb^{3+}, NCMPO:0.04Eu^{2+}, 0.04Mn^{2+}, NCMPO:0.04Eu^{2+}, 0.12Tb^{3+}, 0.01Mn^{2+}, NCMPO:0.01Dy^{3+}, and the standard card for $Na_{18}Ca_{13}Mg_5(PO_4)_{18}$ (JCPDS no. 88-1548).

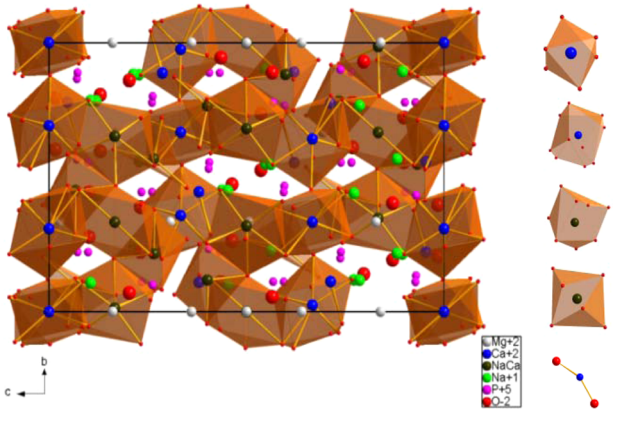

Figure 2. Crystal structure of $Na_{18}Ca_{13}Mg_5(PO_4)_{18}$ compound.

dx.doi.org/10.1021/ic502058r | Inorg. Chem. 2014, 53, 12141−12150

cell parameters of a = 15.811 Å, c = 21.499 Å, V = 4643.62 Å^3, Z = 3.[10] The composition was fixed under the assumption of two cationic positions per phosphorus atom leading to the general formula $NaM^{II}PO4$. Furthermore, there are five Ca cationic positions of Ca1 with Wyckoff position 3a, Ca2 with Wyckoff position 18f, Ca3/Na3 with Wyckoff position 18g, Ca4/Na4 with Wyckoff position 18h, Ca6 with Wyckoff position 18h for Eu^{2+} ions substitution, in which two of them share the same positions with Na cations. Moreover, Ca1 and Ca4 are coordinated with six oxygen atoms around, while 10 for Ca2, 8 for Ca3, and 2 for Ca6. Also, the Eu^{2+}, Tb^{3+}, and Dy^{3+} are suggested to substitute Ca^{2+} based on the similar ionic radius of them [coordination number (CN) = 6, r = 1.00 Å, CN = 8, r = 1.12 Å, CN = 10, r = 1.28 Å for Ca^{2+}; CN = 6, r = 1.17 Å, CN = 8, r = 1.25 Å for Ca^{2+}; CN = 6, r = 0.92 Å, CN = 8, r = 1.04 Å for Tb^{3+}; CN = 6, r = 0.91 Å, CN = 8, r = 1.02 Å for Dy^{3+}], as well as the occupation of Mg^{2+} by Mn^{2+} (CN = 6, r = 0.72 Å, CN = 8, r = 0.89 Å for Mg^{2+}; CN = 6, r = 0.67 Å, CN = 8, r = 0.93 Å for Mn^{2+}). Some small shifts in the diffraction patterns relative to the standard diffraction pattern of JCPDS no. 88-1548 can be ascribed to the differences of ionic radius between Ca^{2+} and Eu^{2+}, Dy^{3+} and Tb^{3+}, as well as between Mg^{2+} and Mn^{2+}.

In order to further identify the effect to crystal structure of doping rare earth ions, the Rietveld refinement of powder XRD profile of representative NCMPO:0.04Eu^{2+} was defined by the general structure analysis system (GSAS) method. The original structure model of previously reported crystallographic data of $Na_{18}Ca_{13}Mg_5(PO_4)_{18}$ (ICSD no. 408372), which crystallizes in a trigonal unit cell with the space group $R\bar{3}m$ (166) was employed to refine the structure of NCMPO:0.04Eu^{2+}. The experimental, calculated, and difference XRD profiles and Bragg positions for the Rietveld refinement of NCMPO:0.04Eu^{2+} at room temperature are shown in Figure 3. The refined results

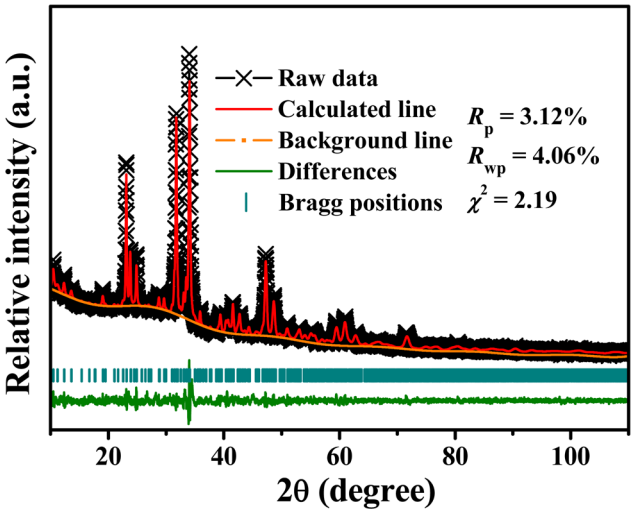

Figure 3. Rietveld refinement of powder XRD profile of representative NCMPO:0.04Eu^{2+}.

show that all atom coordinates, fraction factors, as well as thermal vibration parameters are fitted well with the reflection condition, R_p = 3.12%, R_{wp} = 4.06%, and χ^2 = 2.19, indicating that the introduction of rare earth ions has little influence to the crystal structure of $Na_{18}Ca_{13}Mg_5(PO_4)_{18}$.

XPS was used to determine the elemental compositions of the samples. The measured results of NCMPO and NCMPO:0.04Eu^{2+}, 0.12Tb^{3+}, 0.005Mn^{2+} are illustrated in Figure S1 in the Supporting Information, showing the almost identical profiles and peak positions for binding energies below 600 eV. The doped elements, Eu, Tb, and Mn, were detected in the spectrum of NCMPO:0.04Eu^{2+}, 0.12Tb^{3+}, 0.005Mn^{2+} in Figure S1b in the Supporting Information compared to that of NCMPO host in Figure S1a in the Supporting Information. As illustrated in insets b-1 and b-2 in Figure S1b, the Eu $^3d_{3/2}$, $^3d_{5/2}$ and Mn $^2p_{1/2}$, $^2p_{3/2}$ core peaks show binding energies of around 1166, 1135 eV and 650, 640 eV,[11] respectively, but have weak intensities owing to their low doping concentrations. While for the Tb element, its 4d core peak is observed obviously from inset b-3 in Figure S1b. By combining the result with the XRD analysis, we can infer that these signals originate from elements present in NCMPO and NCMPO:0.04Eu^{2+}, 0.12Tb^{3+}, 0.005Mn^{2+}.

3.2. Photoluminescence Properties. Figure 4 shows the PL emission and excitation spectra of NCMPO:0.04Eu^{2+},

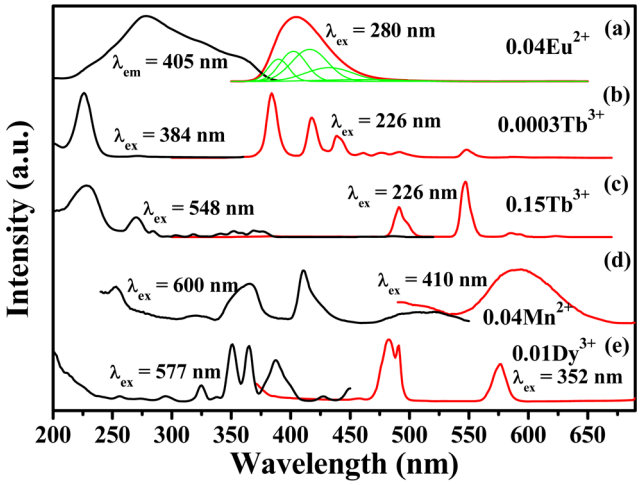

Figure 4. Excitation (black line) and emission (red line) spectra for NCMPO:0.04Eu^{2+} (a), NCMPO:0.0003Tb^{3+} (b), NCMPO:0.15Tb^{3+} (c), NCMPO:0.04Mn^{2+} (d), and NCMPO:0.01Dy^{3+} (e).

NCMPO:0.0003Tb^{3+}, NCMPO:0.15Tb^{3+}, NCMPO:0.04Mn^{2+}, and NCMPO:0.01Dy^{3+} samples at room temperature. In Figure 4a, the PL excitation spectrum has a broad band ranging from 210 to 380 nm monitored at 405 nm with the maximum at about 280 nm, which is ascribed to the $4f^7 \rightarrow 4f^65d^1$ transition of the Eu^{2+} ion and in accordance with the absorption band displayed in the diffuse reflection spectrum of NCMPO:0.04Eu^{2+} in Figure S2 in the Supporting Information. Under 280 nm excitation, the PL emission spectrum of NCMPO:0.04Eu^{2+} shows a purple-blue emission in the region of 375 to 485 nm, peaking at 405 nm, with the full width at half-maximum (fwhm) of about 50 nm, which can be assigned to the typical $4f^65d^1 \rightarrow 4f^7$ transition of the Eu^{2+} ion. On the basis of five kinds of Ca sites in the host, the PL emission spectrum of the NCMPO:0.04Eu^{2+} phosphor can be decomposed into five Gaussian bands with peaks centered at 389, 401, 415, 433, and 464 nm by Gaussian deconvolution, respectively. Figure 5a displays the variation of emission spectra (λ_{ex} = 280 nm) for NCMPO:$x$$Eu^{2+}$ as a function of Eu^{2+} concentration x, one can clearly find that the optimal doping concentration x of Eu^{2+} in this host is 0.04 in Figure 5b, beyond which the concentration quenching effect takes place owing to the energy transfer between activators until an energy

dx.doi.org/10.1021/ic502058r | Inorg. Chem. 2014, 53, 12141−12150

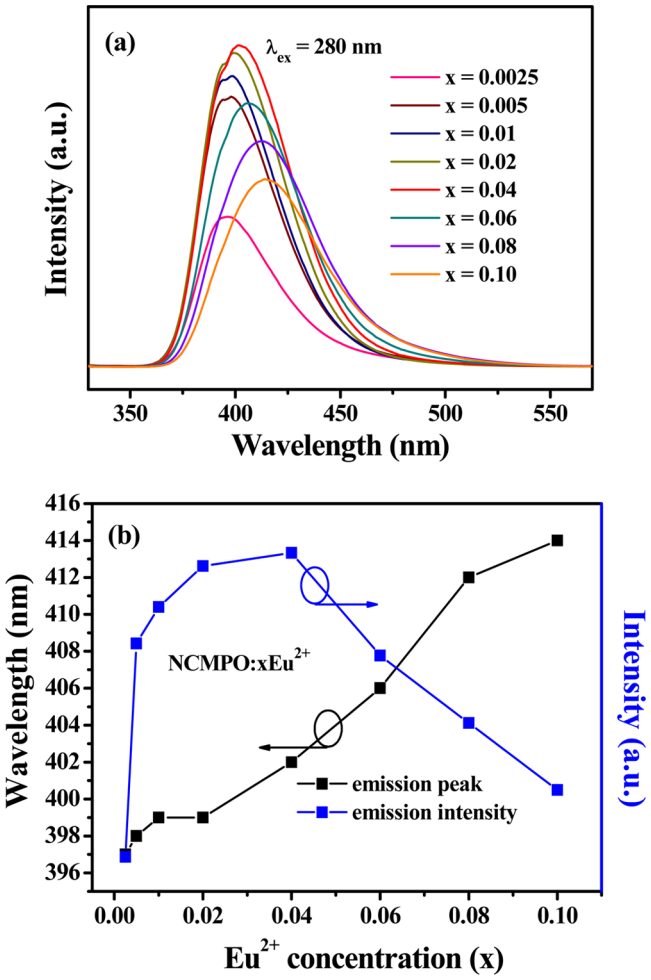

Figure 5. (a) Variation of emission spectra (λ_{ex} = 280 nm) for NCMPO:xEu^{2+} as a function of Eu^{2+} concentration x. (b) Dependence of emission intensity and wavelength of emission peaks on Eu^{2+} concentration.

saturation and then results in the decrease of emission intensity. In order to determine the energy transfer mechanism in NCMPO:xEu^{2+} samples, it is necessary to know the critical distance (R_c) between activators such as Eu^{2+} here. With the increase of Eu^{2+} content, the distance between Eu^{2+} ions becomes shorter, thus the probability of energy migration increases constantly. When the distance is small enough, the concentration quenching occurs and the energy migration is hindered. Therefore, the calculation of R_c has been pointed out by Blasse:[12]

$$R_c \approx 2\left[\frac{3V}{4\pi X_c N}\right]^{1/3} \quad (1)$$

where V corresponds to the volume of the unit cell, N is the number of host cations in the unit cell, and X_c is the critical concentration of dopant ions. For the $Na_{18}Ca_{13}Mg_5(PO_4)_{18}$ host, N = 3, V = 4643.62 Å^3, and X_c is 0.04 × 18 = 0.72 for Eu^{2+}. Accordingly, the R_c was estimated to be about 16.01 Å. In general, there are three mechanisms for nonradiate energy transfer involving exchange interaction, radiation reabsorption, and electric multipolar interactions. The result obtained above indicates the little possibility of exchange interaction since the exchange interaction is predominant only for about 5 Å.[13] The mechanism of radiation reabsorption is only efficacious when the fluorescence and absorption spectra are widely overlapping, which also does not intend to occur in this case. Consequently, we can conclude the energy transfer mechanism between Eu^{2+} ions is appropriate for electric multipolar interactions. According to the formula proposed by Dexter and Van Uitert, which can be expressed as follow:[13a,14]

$$\frac{I}{x} = [1 + \beta(x)^{\theta/3}]^{-1} \quad (2)$$

where I represents the emission intensity, x is the activator ion concentration, and β is a constant for the given matrix under the identical excitation conditions. The type of energy transfer mechanism of electric multipolar interactions can be estimated by analyzing the constant θ from this formula. The value of θ is 6, 8, 10, corresponding to electric dipole-dipole (d-d), dipole-quadrupole (d-q), or quadrupole-quadrupole (q-q) interactions, respectively. The curve of $\log(I/x)$ versus $\log(x)$ in NCMPO:Eu^{2+} phosphors beyond the quenching content of Eu^{2+} is plotted in Figure 6 to determine the value of θ, which

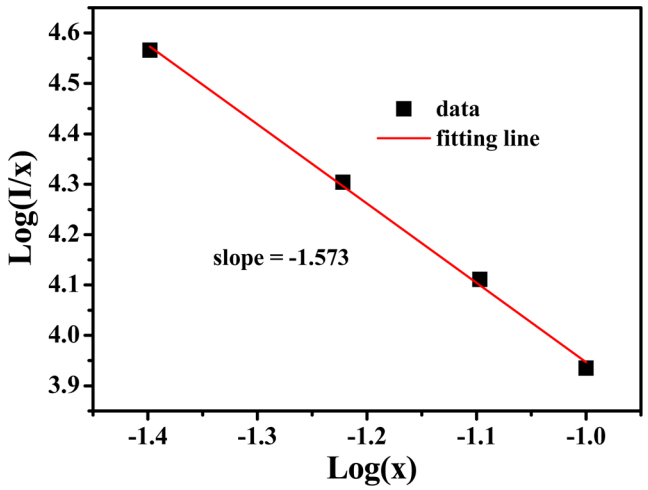

Figure 6. Linear fitting of $\log(x)$ versus $\log(I/x)$ for the various Eu^{2+} singly doped NCMPO phosphors, where I and x are the emission intensity and activator concentration, respectively.

shows a fitted straight line with the slope equal to −1.573 = $-\theta/3$, as a consequence, the θ is approximately 6,[9b,15] indicating the d-d interaction dominates the energy transfer mechanism between Eu^{2+} in NCMPO:Eu^{2+} phosphors. It also can be observed that the emission wavelength produces a red-shift phenomenon under a fixed excitation wavelength of 280 nm in Figure 5b owing to the increase of magnitude of the crystal field (resulting from the constant deduction of distance between Eu^{2+} and O^{2-} when Ca^{2+} is substituted by the larger Eu^{2+} ion), which often similarly takes place in other phosphors.[16]

Figure 4b shows the emission and excitation spectra of low Tb^{3+} doping concentration NCMPO:0.0003Tb^{3+} sample. The excitation spectrum monitored at characteristic emission (384 nm) of Tb^{3+} primarily presents a broad band centered at 226 nm, which is attributed to the spin-allowed transition from the 4f to the 5d state of Tb^{3+}. Compared with NCMPO:0.0003Tb^{3+} sample, the excitation spectrum of the high Tb^{3+} doping concentration NCMPO:0.15Tb^{3+} sample monitored at its unique emission (548 nm) contains many lines besides a broad band centered at 226 nm in Figure 4c, which

dx.doi.org/10.1021/ic502058r | Inorg. Chem. 2014, 53, 12141−12150

correspond to the absorption of the spin-forbidden 4f-4f and spin-allowed 4f-5d transitions of Tb^{3+}, respectively. It is obvious that the NCMPO:Tb^{3+} phosphors can be optimally excited under 226 nm UV radiation. The emission spectra of both NCMPO:0.0003Tb^{3+} and NCMPO:0.15Tb^{3+} consist of the $^5D_{3,4} \rightarrow {}^7F_{J(=6,5,4,3,2)}$ transitions of Tb^{3+} ions, while the primary emission lines are different. The energy difference between $^5D_3$ and $^5D_4$ is close to that between $^7F_0$ and $^7F_6$, which sometimes corresponds to the energy transfer of identical centers: $^5D_3$ (Tb^{3+}) + $^7F_6$ (Tb^{3+}) → $^5D_4$ (Tb^{3+}) + $^7F_0$ (Tb^{3+}).[17] As shown in Figure 7a, with the increase of Tb^{3+} concentration, the emission

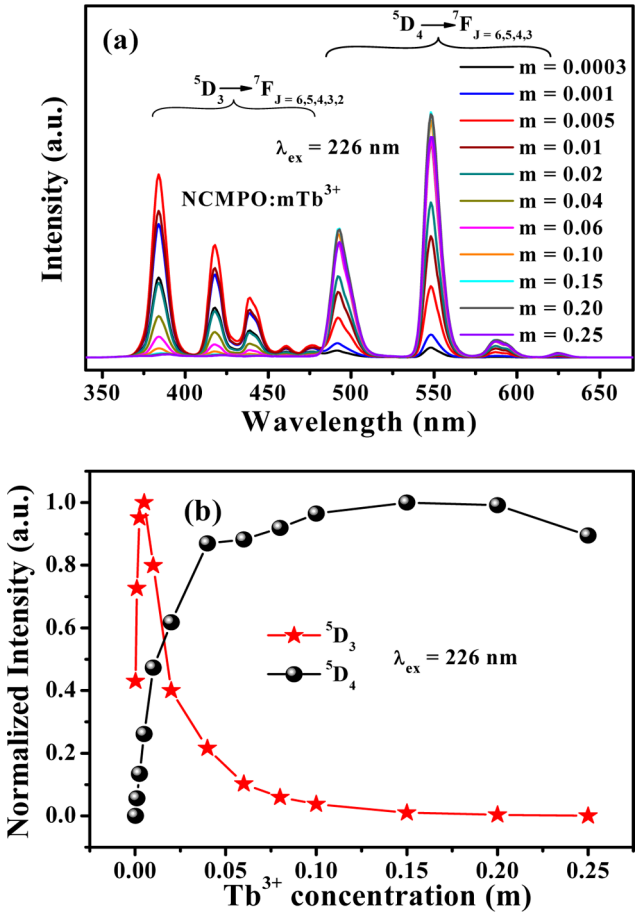

Figure 7. (a) Emission spectra (λ_{ex} = 226 nm) for NCMPO:$m$$Tb^{3+}$ as a function of Tb^{3+} concentration m. (b) Dependence of emission intensities for $^5D_3$ and $^5D_4$ in NCMPO:$m$$Tb^{3+}$ on Tb^{3+} concentration.

spectra show different ratios between the $^5D_3$ and $^5D_4$ emissions. In the emission spectra for low doping concentrations ($m \leq 0.01$), the $^5D_3 \rightarrow {}^7F_{J(=6,5,4,3,2)}$ transitions are predominant, while the $^5D_4 \rightarrow {}^7F_5$ transition at 548 nm is dominant at higher doping concentrations ($m > 0.01$). The emission intensity of $^5D_3$ first increases to a maximum corresponding to the Tb^{3+} concentration m = 0.005 and begins to decrease with further Tb^{3+} concentration owing to the cross-relaxation between the $^5D_3$-$^5D_4$ and $^7F_0$-$^7F_6$ of the two neighboring Tb^{3+}, whereas the emission intensity of $^5D_4$ consecutively increases to high Tb^{3+} concentration m = 0.15 and subsequently decreases attributed to general concentration quenching effect in Figure 7b. The concentration quenching of luminescence is originated from the energy migration among the activator ions at the high concentrations. In the energy migration process, the excitation energy will be lost at a killer or quenching site, resulting in the decrease of PL intensity.[18]

The PL emission and excitation spectra of Mn^{2+} doped NCMPO:0.04Mn^{2+} phosphor are displayed in Figure 4d. The excitation spectrum contains two primary peaks centered at 370 and 410 nm, which correspond to the transitions from $^6A_1$ (^6S) to $^4T_2$ (^4D) and [$^4A_1$ (^4G), ^4E (^4G)] of Mn^{2+}, respectively.[19] It is clearly observed that there is a spectral overlap between the excitation band peaking at 410 nm of Mn^{2+} and the emission band centered at 405 nm of Eu^{2+}, from which we can deduce that the energy transfer from Eu^{2+} to Mn^{2+} ions is able to occur. The emission spectrum of Mn^{2+} excited at 410 nm presents a broad band extending from 540 to 650 nm centered at 600 nm, corresponding to a red emission color.

Figure 4e illustrates the PL emission and excitation spectra of NCMPO:0.01Dy^{3+} sample. The excitation spectrum includes several lines in the range of 250−450 nm originating from characteristic f-f transitions of Dy^{3+} within its $4f^9$ configuration, namely, $^6H_{12/5}$−$^4F_{5/2}$ (328 nm), $^6H_{12/5}$−$^6P_{5/2}$ (352 nm), $^6H_{12/5}$−$^6P_{7/2}$ (368 nm), $^6H_{12/5}$−$^4F_{7/2}$ (385 nm), $^6H_{12/5}$−$^4G_{11/2}$ (428 nm), respectively.[20] The emission spectrum excited at 352 nm presents its characteristic emission lines peaking at 483 and 577 nm, which are originated from Dy^{3+} transitions of $^4F_{9/2}$ to $^6H_{15/2}$ and $^4F_{9/2}$ to $^6H_{13/2}$, respectively. It is well-known that the Dy^{3+} emission around 483 nm ($^4F_{9/2}$−$^6H_{15/2}$) derives from its magnetic dipole transition and the emission around 577 nm ($^4F_{9/2}$−$^6H_{13/2}$) originates from its electric dipole origin. It is observed that the $^4F_{9/2}$−$^6H_{15/2}$ transition is dominant in this host, which implies that Dy^{3+} ions locates at low-symmetry sites with no inversion centers.[21] The emission spectra (λ_{ex} = 352 nm) and the variation of emission intensity for NCMPO:$n$$Dy^{3+}$ with various Dy^{3+} concentration n are shown in Figure S3 in the Supporting Information. We can find that the optimal doping concentration of Dy^{3+} n is 0.01, beyond which the concentration quenching similar to above also occurs, resulting in the decrease of emission intensity.

It is well accepted that Eu^{2+} can serve as a sensitizer to transfer its absorption energy to an activator in certain hosts.[22] In this NCMPO:Eu^{2+}, Tb^{3+}/Mn^{2+} system, the Eu^{2+} can act as a sensitizer to enhance the emission intensity of Tb^{3+} or Mn^{2+}, therefore, resulting in the tunable emission color in codoped samples under UV excitation. Figure 8a,c displays the normalized excitation spectra of NCMPO:0.04Eu^{2+}, 0.12Tb^{3+} (monitored at 405 and 548 nm) and NCMPO:0.04Eu^{2+}, 0.04Mn^{2+} (monitored at 405 and 610 nm). For the NCMPO:0.04Eu^{2+}, 0.12Tb^{3+} sample, the excitation spectrum for Tb^{3+} $^5D_4 \rightarrow {}^7F_5$ transition (548 nm) comprises bands of both Tb^{3+} (220−240 nm) and Eu^{2+} (240−380 nm), the occurrence of Eu^{2+} excitation spectrum indicates the existence of energy transfer from Eu^{2+} to Tb^{3+} ions. Differently, the excitation spectrum for Mn^{2+} $^4T_1 \rightarrow {}^6A_1$ transition (610 nm) is normally identical to that of Eu^{2+}, which reveals that Mn^{2+} ions are essentially excited via Eu^{2+} ions and gives a confirmation of energy transfer from Eu^{2+} to Mn^{2+} ions in the NCMPO:0.04Eu^{2+}, 0.04Mn^{2+} sample. The emission spectra for NCMPO:0.04Eu^{2+}, $y$$Tb^{3+}$ (y = 0−0.28) and NCMPO:0.04Eu^{2+}, $z$$Mn^{2+}$ (z = 0−0.06) under 365 nm UV excitation are illustrated in Figure 8b,d. The emission intensities for Eu^{2+} in NCMPO:0.04Eu^{2+}, $y$$Tb^{3+}$ and NCMPO:0.04Eu^{2+}, $z$$Mn^{2+}$ both decrease monotonously with increasing Tb^{3+} or Mn^{2+} doping concentration, while the emission intensity for Tb^{3+} or Mn^{2+} first increases to a maximum and then decreases

dx.doi.org/10.1021/ic502058r | Inorg. Chem. 2014, 53, 12141−12150

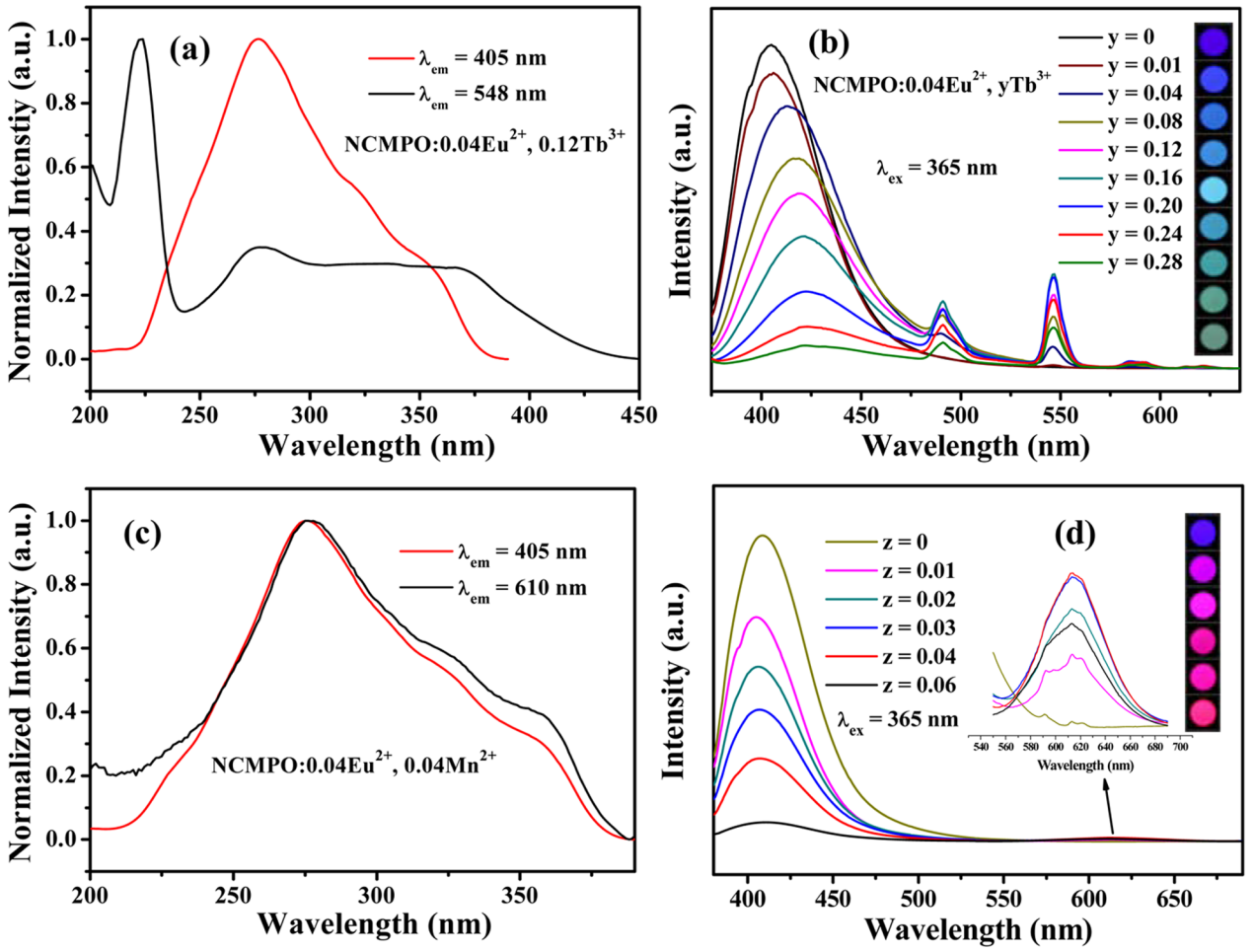

Figure 8. Excitation spectra for NCMPO:0.04Eu^{2+}, 0.12Tb^{3+} (a) and NCMPO:0.04Eu^{2+}, 0.04Mn^{2+} (c) samples. The emission spectra (λ_{ex} = 365 nm) for NCMPO:0.04Eu^{2+}, $y$$Tb^{3+}$ (b) and NCMPO:0.04Eu^{2+}, $z$$Mn^{2+}$ (d) with corresponding digital luminescent photographs on the right under a 365 nm UV lamp excitation.

because of the concentration quenching effect, which further certifies the energy transfer from Eu^{2+} to Tb^{3+} or Mn^{2+} ions, respectively. The corresponding digital photographs under a 365 nm UV lamp excitation are presented on the right of Figure 8b,d, respectively, which show the tunable emission color (purple-blue to green for NCMPO:Eu^{2+}, Tb^{3+} and purple-blue to red for NCMPO:Eu^{2+}, Mn^{2+}) takes place in both systems.

Additionally, the fluorescent decay lifetimes (τ) of Eu^{2+} in NCMPO:Eu^{2+}, Tb^{3+} and NCMPO:Eu^{2+}, Mn^{2+} with various doping concentration of Tb^{3+} or Mn^{2+} are presented in parts a and b of Figure S4 in the Supporting Information, respectively. With the increases of Tb^{3+} or Mn^{2+} concentration, the effective fluorescent decay lifetime of Eu^{2+} ions can be approximately calculated as follows:[23]

$$\tau = \int_0^\infty I(t)\,\mathrm{d}t \tag{3}$$

where τ is calculated lifetime value and $I(t)$ is the normalized intensity of emission spectra. The lifetimes are evaluated to be 159.6, 122.2, 110.8, 72.3 ns corresponding to y = 0, 0.08, 0.20, 0.28 in NCMPO:0.04Eu^{2+}, $y$$Tb^{3+}$ and 159.6, 135.7, 122.2, 95.1 ns corresponding to z = 0, 0.02, 0.04, 0.06 in NCMPO:0.04Eu^{2+}, $z$$Mn^{2+}$ phosphors, respectively. The constant decreases of effective fluorescent lifetimes of Eu^{2+} ions in NCMPO:Eu^{2+}, Tb^{3+}/Mn^{2+} samples with the increases of Tb^{3+} or Mn^{2+} doping concentration further testify the existence of energy transfer from Eu^{2+} to Tb^{3+} or Mn^{2+} ions in NCMPO hosts. Generally, the energy transfer efficiency (η_T) from the sensitizer to the activator could be determined by the following expression:[24]

$$\eta_T = 1 - \frac{I}{I_0} \tag{4}$$

where I_{S0} and I_S are the luminescence intensities of the sensitizer with the absence and presence of the activators, respectively. In this host, the Eu^{2+} can be the sensitizer and the Tb^{3+} or Mn^{2+} ions act as the activators, respectively. The energy transfer efficiencies from Eu^{2+} to Tb^{3+} or Mn^{2+} in this host are calculated as a function of Tb^{3+} or Mn^{2+} doping concentration, which are, respectively, shown in Figure 9a,b. The energy transfer efficiency increases constantly with the increase of Tb^{3+} or Mn^{2+} doping concentration, which can reach about 92.7% and 93.7%, respectively.

As described above, for this host, the R_c is calculated to be 9.70 and 13.99 Å via using eq 1, respectively, where the different value of X_c is defined as the critical concentration of dopant ions (total concentration of Eu^{2+} and Tb^{3+} or Mn^{2+}, approximately 0.18 or 0.06), that is, at which the luminescence intensity of Eu^{2+} is half of that in the sample without Tb^{3+} or Mn^{2+}. Since the value of R_c is much longer than 3−4 Å,[25] which implies the exchange interaction would not be responsible for

dx.doi.org/10.1021/ic502058r | Inorg. Chem. 2014, 53, 12141−12150

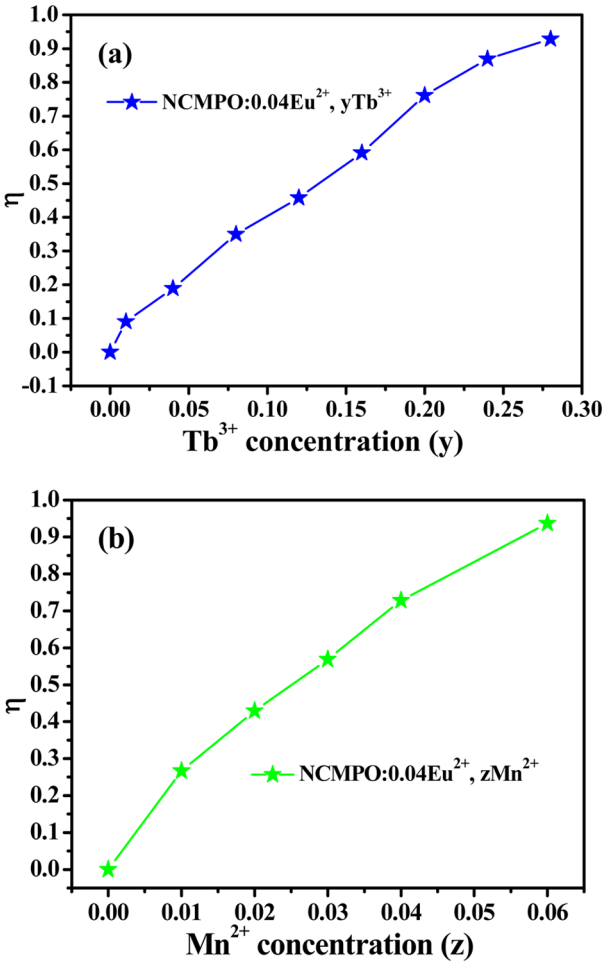

Figure 9. Dependence of the energy transfer efficiency η_T on y (a) and z (b) (λ_{ex} = 365 nm).

the energy transfer mechanism from Eu^{2+} to Tb^{3+} or Mn^{2+} ions. As a result, we can infer that the electric multipolar interactions will take place for energy transfer from Eu^{2+} to Tb^{3+} or Mn^{2+} ions. On account of Dexter's energy transfer formula of multipolar interaction and Reisfeld's approximation, the following relationship can be attained:[26]

$$\frac{\eta_{S0}}{\eta_S} \propto C^{\alpha/3} \quad (5)$$

where η_{S0} and η_S represent the luminescence quantum efficiencies of the Eu^{2+} ions with the absence and presence of the Tb^{3+} or Mn^{2+} ions, respectively. C is Mn^{2+} and the total concentration of the Eu^{2+} and Tb^{3+} ions. The value for α = 6, 8, and 10 corresponds to d-d, d-q, and q-q interactions, respectively. However, the value of η_{S0}/η_S is hard to be obtained and therefore it can be approximately calculated instead by the I_{S0}/I_S, where I_{S0} and I_S stand for the luminescence intensity of the Eu^{2+} ions without and with the Tb^{3+} or Mn^{2+} ions, respectively. Consequently, the following relation can be obtained:

$$\frac{I_{S0}}{I_S} \propto C^{\alpha/3} \quad (6)$$

The relationships between I_{S0}/I_S and $C^{\alpha/3}$, which are fitted using, respectively, straight lines and based on the above equation, are illustrated in Figure S5 in the Supporting Information. One can find that the biggest R^2 of the linear fitting is when α = 10 and 8 in parts a and b of Figure S5 in the Supporting Information, respectively, which indicates that these relationships are considered to be the best linear behaviors when α = 10 and 8, respectively. Therefore, the energy transfer from Eu^{2+} to Tb^{3+} or Mn^{2+} ions takes place through the q-q and d-q interactions mechanism in NCMPO:Eu^{2+}, Tb^{3+} and NCMPO:Eu^{2+}, Mn^{2+} phosphors, respectively.

On the basis of the efficient energy transfer from Eu^{2+} to Tb^{3+} or Mn^{2+} ions, a series of Eu^{2+}, Tb^{3+}, and Mn^{2+} triply doped phosphors with fixed Eu^{2+} doping concentration have been designed and prepared to acquire expected white emission color in a single-component host. The emission spectra (λ_{ex} = 365 nm) for NCMPO:0.04Eu^{2+}, $y$$Tb^{3+}$, $z$$Mn^{2+}$ (y = 0.08, 0.12, 0.16, z = 0.005, 0.01, 0.02, 0.04) phosphors have been illustrated in Figure S6 in the Supporting Information. It shows that each emission band contains the Eu^{2+}, Tb^{3+}, and Mn^{2+} emission bands, making the samples present different colors including white (observed from the digital luminescent photographs under a 365 nm UV lamp excitation on the right in Figure S6 in the Supporting Information) with the variation of Tb^{3+} and Mn^{2+} concentrations under 365 nm UV excitation.

The quantum yields (QYs) of NCMPO:0.04Eu^{2+}, $y$$Tb^{3+}$, $z$$Mn^{2+}$ samples under 280 nm UV excitation have been measured and listed in Table 1. The maximum value can reach

Table 1. Quantum Yields (QYs) of NCMPO:0.04Eu^{2+}, $y$$Tb^{3+}$, $z$$Mn^{2+}$ Samples under 280 nm UV Excitation

NCMPO:0.04Eu^{2+}, $y$$Tb^{3+}$, $z$$Mn^{2+}$	QY (%)	NCMPO:0.04Eu^{2+}, $y$$Tb^{3+}$, $z$$Mn^{2+}$	QY (%)
y = 0, z = 0	46	y = 0, z = 0.01	33
y = 0.01, z = 0	43	y = 0, z = 0.02	31
y = 0.04, z = 0	54	y = 0, z = 0.04	29
y = 0.08, z = 0	54	y = 0, z = 0.06	12
y = 0.12, z = 0	49	y = 0.08, z = 0.005	49
y = 0.16, z = 0	45	y = 0.08, z = 0.04	39
y = 0.20, z = 0	35	y = 0.12, z = 0.005	46
y = 0.24, z = 0	30	y = 0.12, z = 0.01	47
y = 0.28, z = 0	25	y = 0.12, z = 0.02	44
y = 0.16, z = 0.04	12	y = 0.12, z = 0.04	32

54% for NCMPO:0.04Eu^{2+}, 0.04Tb^{3+}, 33% for NCMPO:0.04Eu^{2+}, 0.01Mn^{2+}, and 49% for NCMPO:0.04Eu^{2+}, 0.08Tb^{3+}, 0.005Mn^{2+}, respectively. Moreover, the QY can be further improved by controlling the morphology, particle size, and crystalline defects via optimizing the synthesis process and chemical composition.

3.3. Cathodoluminescence Properties. In addition, the CL properties of as-synthesized NCMPO:Eu^{2+}/Tb^{3+}/Mn^{2+}, Dy^{3+} samples have been investigated in detail to recognize their potential application in FEDs. Figure 10 illustrates the typical CL spectra (accelerating voltage = 2.5 kV, filament current = 88 mA) together with the corresponding digital luminescent photographs of NCMPO:Eu^{2+}/Tb^{3+}/Mn^{2+}, Dy^{3+} samples. The Eu^{2+}, Tb^{3+}, Mn^{2+}, Dy^{3+} ions in this host can display their, respectively, characteristic emissions under low-voltage electron beam bombardment. All the representative emission spectra are similar to the PL emission spectra, which also give the various emission colors from purple-blue to red observed on the right of Figure 10. The CL spectra for NCMPO:$m$$Tb^{3+}$ (m = 0.005–0.15) phosphors under low-voltage electron beam excitation

dx.doi.org/10.1021/ic502058r | Inorg. Chem. 2014, 53, 12141−12150

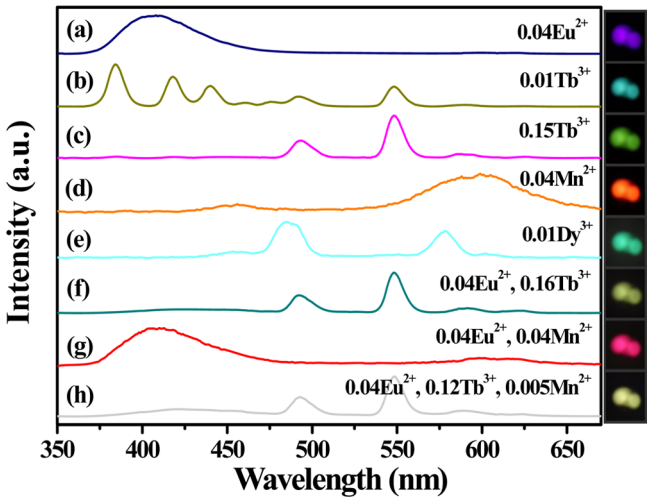

Figure 10. CL spectra for NCMPO:0.04Eu^{2+} (a), NCMPO:0.01Tb^{3+} (b), NCMPO:0.15Tb^{3+} (c), NCMPO:0.04Mn^{2+} (d), NCMPO:0.01Dy^{3+} (e), NCMPO:0.04Eu^{2+}, 0.16Tb^{3+} (f), NCMPO:0.04Eu^{2+}, 0.04Mn^{2+} (g), NCMPO:0.04Eu^{2+}, 0.12Tb^{3+}, 0.005Mn^{2+} (h) with corresponding digital luminescent photographs on the right under low-voltage electron beam excitation.

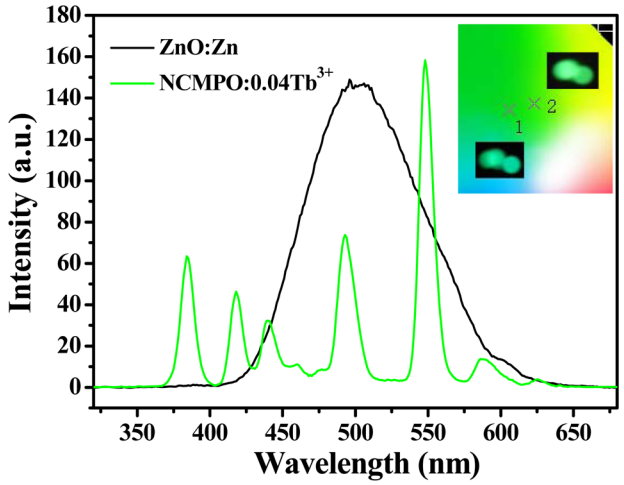

Figure 11. CL spectra of ZnO:Zn and NCMPO:0.04Tb^{3+} under low-voltage electron beam excitation with the accelerating voltage of 3 kV and filament current of 88 mA. The inset is the digital luminescent photographs and CIE coordinates for the phosphors (1, ZnO:Zn; 2, NCMPO:0.04Tb^{3+}).

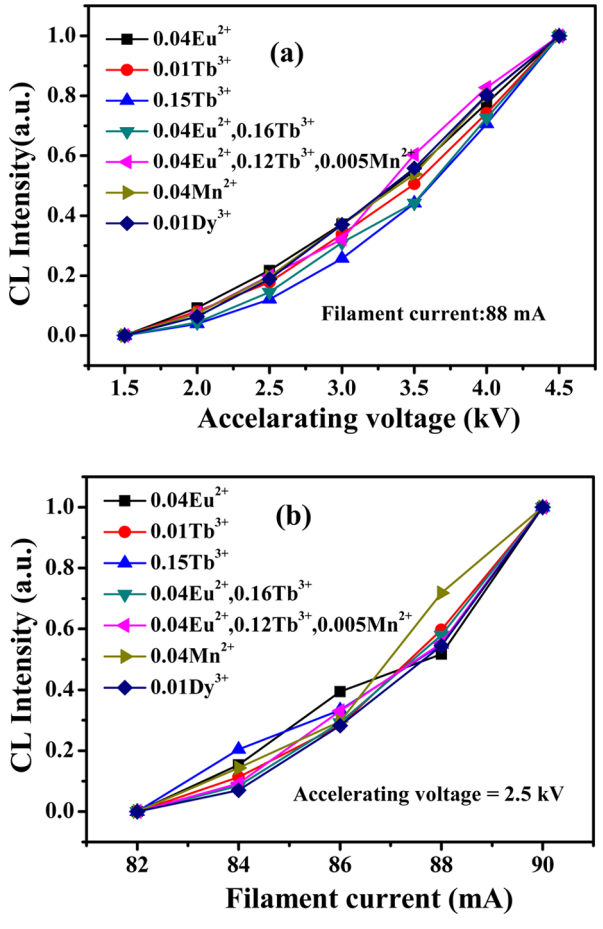

Figure 12. CL intensities of NCMPO:0.04Eu^{2+}, NCMPO:0.01Tb^{3+}, NCMPO:0.15Tb^{3+}, NCMPO:0.04Mn^{2+}, NCMPO:0.01Dy^{3+}, NCMPO:0.04Eu^{2+}, 0.16Tb^{3+}, NCMPO:0.04Eu^{2+}, 0.12Tb^{3+}, and 0.005Mn^{2+} samples as a function of (a) accelerating voltage and (b) filament current.

with the accelerating voltage of 2.5 kV and filament current of 88 mA are presented in Figure S7 in the Supporting Information. One can find that the strongest emission intensity of the $^5D_3 \rightarrow {}^7F_6$ transition at 384 nm is more intense than that of the $^5D_4 \rightarrow {}^7F_5$ transition at 548 nm, which is not identical with the PL spectra. The reason for this observation originates from the different excitation source.[27] For CL, the primary fast and energetic electrons produce many secondary electrons with a very broad excitation energy distribution. Thereby, all these electrons involving primary and secondary electrons can populate both the low-energy states and the high-energy states of activators, which results in the high-energy states of activators more remarkable. It is well-known that the commercial ZnO:Zn displays bright green luminescence and has been demonstrated to be a good candidate for FEDs phosphor under low-voltage excitation. Figure 11 shows the comparison of CL spectra and digital luminescent photographs of ZnO:Zn and NCMPO:0.04Tb^{3+} under low-voltage electron beam excitation with the accelerating voltage of 3 kV and filament current of 88 mA. It can be seen the CL intensity of as-prepared NCMPO:0.04Tb^{3+} (in height) is comparable with that of ZnO:Zn, and the calculated CIE coordinate of NCMPO:0.04Tb^{3+} (0.252, 0.432) is more saturated than it (0.195, 0.417), as presented in Figure 11, indicating that it is a promising candidate for FEDs phosphor.

The variation of CL intensities of representative NCMPO:0.04Eu^{2+}, NCMPO:0.01Tb^{3+}, NCMPO:0.15Tb^{3+}, NCMPO:0.04Mn^{2+}, NCMPO:0.01Dy^{3+}, NCMPO:0.04Eu^{2+}, 0.16Tb^{3+}, NCMPO:0.04Eu^{2+}, 0.12Tb^{3+}, and 0.005Mn^{2+} samples as a function of the accelerating voltage and filament current have been investigated in detail, respectively. At a fixed filament current of 88 mA, the CL intensities of phosphors increase without a saturation with the increase of accelerating voltage from 1.5 to 4.5 kV (Figure 12a). Similarly, with the increasing filament current from 82 to 90 mA at a stationary accelerating voltage of 2.5 kV, the CL intensities of phosphors ascends monotonously (Figure 12b). The raise in CL brightness with an increase in electron energy and filament current can be ascribed to the deeper penetration of the electrons into the phosphors body and the larger electron-beam current density. The electron penetration depth can be evaluated utilizing the empirical formula L [Å] = 250(A/

dx.doi.org/10.1021/ic502058r | Inorg. Chem. 2014, 53, 12141−12150

$\rho)(E/Z^{1/2})^n$, where $n = 1.2/(1-0.29 \log_{10} Z)$, A refers to the atomic or molecular weight of the material, ρ is the bulk density, Z is the atomic number or the number of electrons per molecule in the case compounds, and E is the accelerating voltage (kV).[28] For $Na_{18}Ca_{13}Mg_5(PO_4)_{18}$, $Z = 1364$, $A = 2765.84$, $\rho = 2.97$ g/cm^3. Therefore, the electron penetration depths are estimated to be 85.12 pm, 7.22 nm, and 199.36 nm, corresponding to the accelerating voltages 2.5, 3.5, and 4.5 kV, according to above equation, respectively. For CL, the Eu^{2+}, Tb^{3+}, Mn^{2+}, and Dy^{3+} ions are excited by the plasma produced by the incident electrons. The deeper the electron penetration depth, the more plasma will be produced, which results in more Eu^{2+}, Tb^{3+}, Mn^{2+}, and Dy^{3+} ions being excited, and thus the CL intensity increases.

4. CONCLUSIONS

A succession of NCMPO:A (A = Eu^{2+}/Tb^{3+}/Mn^{2+}, Dy^{3+}) phosphors have been first prepared by the high-temperature solid-state reaction method. The pure crystalline phase of as-prepared samples has been demonstrated via XRD measurement and Rietveld refinements. The NCMPO:A (A = Eu^{2+}/Tb^{3+}/Mn^{2+}) show tunable color from purple-blue to red based on energy transfer from Eu^{2+} to Tb^{3+} or Mn^{2+} ions under UV excitation which are demonstrated by their variations of emission spectra and fluorescent decay curves with the increase of Tb^{3+} or Mn^{2+} content. The maximum value of QY can reach 54% for NCMPO:0.04Eu^{2+}, 0.04Tb^{3+}, 33% for NCMPO:0.04Eu^{2+}, 0.01Mn^{2+}, and 49% for NCMPO:0.04Eu^{2+}, 0.08Tb^{3+}, 0.005Mn^{2+}, respectively. Under low-voltage electron beam bombardment excitation, the NCMPO:A (A = Eu^{2+}/Tb^{3+}/Mn^{2+}, Dy^{3+}) phosphors display their, respectively, characteristic emissions and correspondingly various colors. Importantly, the CL intensity of as-prepared NCMPO:0.04Tb^{3+} (in height) is comparable with that of ZnO:Zn, and the calculated CIE coordinate of NCMPO:0.04Tb^{3+} (0.252, 0.432) is more saturated than it (0.195, 0.417). These results show their potential applied to WLEDs and FEDs.

■ ASSOCIATED CONTENT

Supporting Information

XPS spectra of (a) the NCMPO host and (b) NCMPO:0.04Eu^{2+}, 0.12Tb^{3+}, 0.005Mn^{2+}. Insets show the XPS spectra of the Eu, Tb, Mn elements in NCMPO:0.04Eu^{2+}, 0.12Tb^{3+}, 0.005Mn^{2+} (Figure S1). Diffuse reflection spectra of the NCMPO host and NCMPO:0.04Eu^{2+} samples (Figure S2). Emission spectra (λ_{ex} = 352 nm) for NCMPO:$n$$Dy^{3+}$ with different Dy^{3+} concentration n. Inset is the dependence of emission intensity on Dy^{3+} concentration (Figure S3). Fluorescent decay curves for the luminescence of Eu^{2+} in for NCMPO:0.04Eu^{2+}, $y$$Tb^{3+}$ (a) and NCMPO:0.04Eu^{2+}, $z$$Mn^{2+}$ (b) samples with various Tb^{3+} or Mn^{2+} doping concentrations (Figure S4). Dependence of I_{S0}/I_S of Eu^{2+} on $C_{Eu^{2+}+Tb^{3+}}^{3+6/3}$, $C_{Eu^{2+}+Tb^{3+}}^{3+8/3}$ and $C_{Eu^{2+}+Tb^{3+}}^{3+10/3}$ (a), and $C_{Mn^{2+}}^{2+6/3}$, $C_{Mn^{2+}}^{2+8/3}$ and $C_{Mn^{2+}}^{2+10/3}$ (b) (Figure S5). Emission spectra (λ_{ex} = 365 nm) for NCMPO:0.04Eu^{2+}, $y$$Tb^{3+}$, $z$$Mn^{2+}$ with corresponding digital luminescent photographs on the right under a 365 nm UV lamp excitation (Figure S6). Variation of CL spectra for NCMPO:$m$$Tb^{3+}$ (m = 0.005–0.15) phosphors under low-voltage electron beam excitation with the accelerating voltage of 2.5 kV and filament current of 88 mA (Figure S7). This material is available free of charge via the Internet at http://pubs.acs.org.

■ AUTHOR INFORMATION

Corresponding Authors

*E-mail: jlin@ciac.ac.cn.

*E-mail: hzlian@ciac.ac.cn.

Notes

The authors declare no competing financial interest.

■ ACKNOWLEDGMENTS

This project is financially supported by the National Natural Science Foundation of China (NSFC Grants 51332008, 51172227, 51472234, and 21221061), National Basic Research Program of China (Grants 2010CB327704 and 2014CB643803), and the Joint Funds of the National Natural Science Foundation of China and Guangdong Province (Grant No. U1301242).

■ REFERENCES

(1) (a) Huang, K.-W.; Chen, W.-T.; Chu, C.-I.; Hu, S.-F.; Sheu, H.-S.; Cheng, B.-M.; Chen, J.-M.; Liu, R.-S. *Chem. Mater.* **2012**, *24*, 2220–2227. (b) Lai, S.; Yang, Z.; Wang, R.; Wu, H.; Liao, J.; Qiu, J.; Song, Z.; Yang, Y.; Zhou, D. *J. Mater. Sci.* **2013**, *48*, 8566–8570. (c) Yeh, C.-W.; Chen, W.-T.; Liu, R.-S.; Hu, S.-F.; Sheu, H.-S.; Chen, J.-M.; Hintzen, H. T. *J. Am. Chem. Soc.* **2012**, *134*, 14108–14117. (d) Yu, X.; Zhang, L.; Xu, X.; Wang, T.; Yu, H.; Jiang, T.; Jiao, Q.; Yang, Z.; Zhou, D.; Qiu, J. *J. Lumin.* **2014**, *145*, 114–118. (e) Yang, Z.; Liao, J.; Lai, S.; Wu, H.; Fan, Z.; Qiu, J.; Song, Z.; Yang, Y.; Zhou, D. *Mater. Express* **2013**, *3*, 350–354.

(2) (a) Wen, D.; Shi, J. *Dalton Trans.* **2013**, *42*, 16621–16229. (b) Huang, C.-H.; Chen, T.-M. *Inorg. Chem.* **2011**, *50*, 5725–5730. (c) Shang, M.; Geng, D.; Zhang, Y.; Li, G.; Yang, D.; Kang, X.; Lin, J. *J. Mater. Chem.* **2012**, *22*, 19094–19104. (d) Jin, Y.; Hu, Y.; Chen, L.; Wang, X.; Mu, Z.; Ju, G.; Yang, Z. *Physica B* **2014**, *436*, 105–110.

(3) (a) Liu, X.; Liu, Y.; Yan, D.; Zhu, H.; Liu, C.; Liu, W.; Xu, C.; Liu, Y.; Zhang, H.; Wang, X. *Dalton Trans.* **2013**, *42*, 16311–16317. (b) Han, L.; Zhao, L.; Zhang, J.; Wang, Y.; Guo, L.; Wang, Y. *RSC Adv.* **2013**, *3*, 21824–21831. (c) Li, G.; Zhang, Y.; Geng, D.; Shang, M.; Peng, C.; Cheng, Z.; Lin, J. *ACS Appl. Mater. Interfaces* **2012**, *4*, 296–305.

(4) (a) Lee, K. H.; Choi, S.; Jung, H.-K.; Im, W. B. *Acta Mater.* **2012**, *60*, 5783–5790. (b) Jiao, M.; Guo, N.; Lu, W.; Jia, Y.; Lv, W.; Zhao, Q.; Shao, B.; You, H. *Inorg. Chem.* **2013**, *52*, 10340–10346. (c) Kohale, R. L.; Dhoble, S. J. *J. Alloys Compd.* **2014**, *586*, 314–318. (d) Xia, Z.; Liu, R.-S. *J. Phys. Chem. C* **2012**, *116*, 15604–15609.

(5) (a) Lü, J.; Huang, Y.; Shi, L.; Seo, H. *J. Appl. Phys. A* **2010**, *99*, 859–863. (b) Hou, D.; Chen, W.; Ding, X.; Liang, H.; Zheng, L.; Zhang, J. *ECS J. Solid State Chem.* **2013**, *2*, R79–R81. (c) Kim, J. S.; Song, H. J.; Roh, H.-S.; Yim, D. K.; Noh, J. H.; Hong, K. S. *Mater. Lett.* **2012**, *79*, 112–115. (d) Huang, C.-H.; Wang, D.-Y.; Chiu, Y.-C.; Yeh, Y.-T.; Chen, T.-M. *RSC Adv.* **2012**, *2*, 9130–9134. (e) Piao, X.; Machida, K.; Horikawa, T.; Hanzawa, H.; Shimomura, Y.; Kijima, N. *Chem. Mater.* **2007**, *19*, 4592–4599. (f) Han, J. Y.; Im, W. B.; Kim, D.; Cheong, S. H.; Lee, G.; Jeon, D. Y. *J. Mater. Chem.* **2012**, *22*, 5374–5381.

(6) Zhang, Y.; Kang, X.; Geng, D.; Shang, M.; Wu, Y.; Li, X.; Lian, H.; Cheng, Z.; Lin, J. *Dalton Trans.* **2013**, *42*, 14140–14148.

(7) (a) Haranath, D.; Mishra, S.; Yadav, S.; Sharma, R. K.; Kandpal, L. M.; Vijayan, N.; Dalai, M. K.; Sehgal, G.; Shanker, V. *Appl. Phys. Lett.* **2012**, *101*, 221905. (b) Lu, J.; Du, F.; Zhu, R.; Huang, Y.; Seo, H. J. *J. Mater. Chem.* **2011**, *21*, 16398–16405. (c) Liu, W.-R.; Huang, C.-H.; Yeh, C.-W.; Tsai, J.-C.; Chiu, Y.-C.; Yeh, Y.-T.; Liu, R.-S. *Inorg. Chem.* **2012**, *51*, 9636–9641. (d) Huang, C.-H.; Chan, T.-S.; Liu, W.-R.; Wang, D.-Y.; Chiu, Y.-C.; Yeh, Y.-T.; Chen, T.-M. *J. Mater. Chem.* **2012**, *22*, 20210–20216. (e) Xia, Z.; Zhang, Y.; Molokeev, M. S.; Atuchin, V. V. *J. Phys. Chem. C* **2013**, *117*, 20847–20854.

(8) (a) Zhang, Z.; Mao, Z.; Song, S.; Zhang, J.; Liu, L.; Zhang, W.; Wang, D. *Mater. Lett.* **2013**, *90*, 1–3. (b) Xia, W.; Wang, X.; Fu, Z.; Zhou, S.; Zhang, S.; Jeong, J. H. *Mater. Res. Bull.* **2012**, *47*, 2535–2540.

(9) (a) Guo, N.; Song, Y.; You, H.; Jia, G.; Yang, M.; Liu, K.; Zheng, Y.; Huang, Y.; Zhang, H. *Eur. J. Inorg. Chem.* **2010**, 4636−4642. (b) Song, H. J.; Yim, D. K.; Roh, H.-S.; Cho, I. S.; Kim, S.-J.; Jin, Y.-H.; Shim, H.-W.; Kim, D.-W.; Hong, K. S. *J. Mater. Chem. C* **2013**, *1*, 500−505. (c) Shi, L.; Huang, Y.; Seo, H. J. *J. Phys. Chem. A* **2010**, *114*, 6927−6934. (d) Li, Y.; Li, H.; Liu, B.; Zhang, J.; Zhao, Z.; Yang, Z.; Wen, Y.; Wang, Y. *J. Phys. Chem. Solids* **2013**, *74*, 175−180.
(10) Alkemper, J.; Fuess, H. *Z. Kristallogr.* **1998**, *213*, 282−287.
(11) (a) Zhang, J.; Zhou, M.; Liu, B.; Wen, Y.; Wang, Y. *J. Lumin.* **2012**, *132*, 1949−1952. (b) Létourneau, M.; Tremblay, M.; Faucher, L.; Rojas, D.; Chevallier, P.; Gossuin, Y.; Lagueux, J.; Fortin, M. A. *J. Phys. Chem. B* **2012**, *116*, 13228−13238. (c) Ilyas, U.; Rawat, R. S.; Wang, Y.; Tan, T. L.; Lee, P.; Chen, R.; Sun, H. D.; Li, F.; Zhang, S. *Appl. Surf. Sci.* **2012**, *258*, 6373−6378.
(12) (a) Saradhi, M. P.; Varadaraju, U. V. *Chem. Mater.* **2006**, *18*, 5267−5272. (b) Blasse, G. *Philips Res. Rep.* **1969**, *24*, 131−144. (c) Huang, C.-H.; Chiu, Y.-C.; Yeh, Y.-T.; Chan, T.-S.; Chen, T.-M. *ACS Appl. Mater. Interfaces* **2012**, *4*, 6661−6668.
(13) (a) Dexter, D. L. *J. Chem. Phys.* **1953**, *21*, 836−850. (b) Xia, Z.; Liu, R.-S.; Huang, K.-W.; Drozd, V. *J. Mater. Chem.* **2012**, *22*, 15183−15189. (c) Lv, W.; Jia, Y.; Zhao, Q.; Jiao, M.; Shao, B.; Lü, W.; You, H. *RSC Adv.* **2014**, *4*, 7588−7593.
(14) Van Uitert, L. G. *J. Electrochem. Soc.* **1967**, *114* (10), 1048−1053.
(15) Yu, H.; Deng, D.; Xu, S.; Yu, C.; Yin, H.; Nie, Q. L. *J. Lumin.* **2012**, *132*, 2553−2556.
(16) (a) Lee, G.; Han, J. Y.; Im, W. B.; Cheong, S. H.; Jeon, D. Y. *Inorg. Chem.* **2012**, *51*, 10688−10694. (b) Wen, D.; Dong, Z.; Shi, J.; Gong, M.; Wu, M. *ECS J. Solid State Sci. Technol.* **2013**, *2*, R178−R185. (c) Park, W. B.; Singh, S. P.; Yoon, C.; Sohn, K.-S. *J. Mater. Chem.* **2012**, *22*, 14068−14075.
(17) (a) Sohn, K.-S.; Choi, Y. Y.; Park, H. D.; Choi, Y. G. J. *J. Electrochem. Soc.* **2000**, *147*, 2375−2379. (b) Sohn, K.-S.; Shin, N. *Electrochem. Solid-State Lett.* **2002**, *5*, H21−H23.
(18) Blasse, G.; Grabmaier, B. C. *Luminescence Materials*; Springer-Verlag: Berlin, Heidelberg, Germany, 1994.
(19) (a) Song, E.; Zhao, W.; Zhou, G.; Dou, X.; Ming, H.; Yi, C. *Curr. Appl. Phys.* **2011**, *11*, 1374−1378. (b) Sun, J.; Lian, Z.; Shen, G.; Shen, D. *RSC Adv.* **2013**, *3*, 18395−18405.
(20) (a) Rui, Z.; Xiang, W. *J. Alloys Compd.* **2011**, *509*, 1197−1200. (b) Liu, Q.; Liu, Y.; Yang, Z.; Han, Y.; Li, X.; Fu, G. *J. Alloys Compd.* **2012**, *515*, 16−19. (c) Shang, M.; Geng, D.; Yang, D.; Kang, X.; Zhang, Y.; Lin, J. *Inorg. Chem.* **2013**, *52*, 3102−3112.
(21) (a) Su, Q.; Pei, Z.; Chi, L.; Zhang, H.; Zou, F. *J. Alloys Compd.* **1993**, *192*, 25−27. (b) Su, Q.; Pei, Z.; Lin, J.; Xue, F. *J. Alloys Compd.* **1995**, *225*, 103−106.
(22) (a) Tang, W.; Fu, T.; Deng, K.; Wu, M. *Ceram. Int.* **2013**, *39*, 6363−6367. (b) Lü, W.; Zhang, X.; Wang, Y.; Hao, Z.; Liu, Y.; Luo, Y.; Wang, X.; Zhang, J. *J. Alloys Compd.* **2012**, *513*, 430−435.
(23) (a) Liu, Y.; Zhang, X.; Hao, Z.; Luo, Y.; Wang, X.; Zhang, J. *J. Mater. Chem.* **2011**, *21*, 16379−16384. (b) Hou, D.; Liu, C.; Ding, X.; Kuang, X.; Liang, H.; Sun, S.; Huang, Y.; Tao, Y. *J. Mater. Chem. C* **2013**, *1*, 493−499.
(24) (a) Yang, W. J.; Chen, T. M. *Appl. Phys. Lett.* **2006**, *88*, 101903. (b) Paulose, P. I.; Jose, G.; Thomas, V.; Unnikrishnan, N. V.; Warrier, M. K. R. *J. Phys. Chem. Solids* **2003**, *64*, 841−846.
(25) (a) Jiang, T.; Yu, X.; Xu, X.; Yu, H.; Zhou, D.; Qiu, J. *Mater. Res. Bull.* **2014**, *51*, 80−84. (b) Liu, H.; Liao, L.; Xia, Z. *RSC Adv.* **2014**, *4*, 7288−7295.
(26) (a) Biju, P. R.; Jose, G.; Thomas, V.; Nampoori, V. P. N.; Unnikrishnan, N. V. *Opt. Mater.* **2004**, *24*, 671−677. (b) Dexter, D. L.; Schulman, J. H. *J. Chem. Phys.* **1954**, *22*, 1063−1070.
(27) Zhu, G.; Ci, Z.; Wang, Q.; Wen, Y.; Han, S.; Shi, Y.; Xin, S.; Wang, Y. *J. Mater. Chem. C* **2013**, *1*, 4490−4496.
(28) Feldman, C. *Phys. Rev.* **1960**, *117*, 455−457.